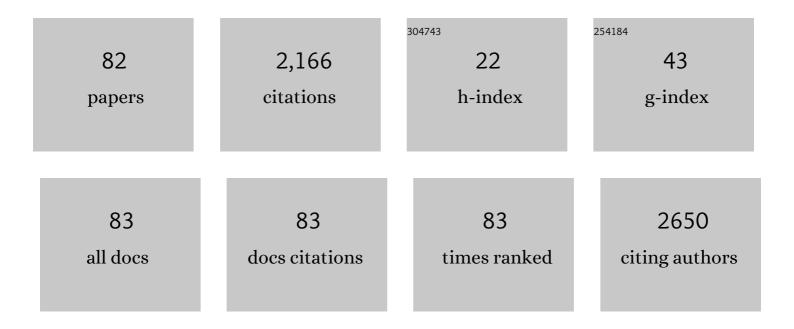
å©·å©· å¼

List of Publications by Year in descending order

Source: https://exaly.com/author-pdf/337723/publications.pdf Version: 2024-02-01



#	Article	IF	CITATIONS
1	Interfacial bonding characteristics and mechanical properties of H68/AZ31B clad plate. International Journal of Minerals, Metallurgy and Materials, 2022, 29, 1237-1248.	4.9	2
2	Effect of Spinning Deformation on Microstructure Evolution and Mechanical Properties of Al-Zn-Mg-Cu (7075) Alloy. Journal of Materials Engineering and Performance, 2022, 31, 6473-6486.	2.5	5
3	Controlled Synthesis of Mesoporous <i>ï€</i> â€Conjugated Polymer Nanoarchitectures as Anodes for Lithiumâ€ion Batteries. Macromolecular Rapid Communications, 2022, 43, e2100897.	3.9	4
4	Interfacially responsive electron transfer and matter conversion by polydopamineâ€mediated nanoplatforms for advancing disease theranostics. Wiley Interdisciplinary Reviews: Nanomedicine and Nanobiotechnology, 2022, 14, e1805.	6.1	3
5	Low-cost and advanced symmetry supercapacitors based on three-dimensional tea waste of porous carbon nanosheets. Materials Technology, 2021, 36, 1-10.	3.0	13
6	Tak1 in the astrocytes of mediobasal hypothalamus regulates anxietyâ€like behavior in mice. Glia, 2021, 69, 609-618.	4.9	6
7	Distributed Real-time State Estimation for Combined Heat and Power Systems. Journal of Modern Power Systems and Clean Energy, 2021, 9, 316-327.	5.4	25
8	One-step microwave-assisted solvothermal nano-manufacturing of Ni2P nanosphere as high-performance supercapacitors. Ionics, 2021, 27, 801-810.	2.4	13
9	Mechanical Characterization of The Plastic Deformation Behavior of AZ31 Magnesium Alloy Processed Through Spinning Using Nanoindentation. Transactions of the Indian Institute of Metals, 2021, 74, 1349-1359.	1.5	4
10	An accurate parameter extraction method for small signal model of CNFET. International Journal of Numerical Modelling: Electronic Networks, Devices and Fields, 2021, 34, e2896.	1.9	0
11	One-step synthesis of ultra-high aspect ratio silver nanowires for high-performance flexible transparent conductive films. Journal of Materials Science: Materials in Electronics, 2021, 32, 15622-15632.	2.2	6
12	Microstructure and Mechanical Properties of AZ31B Magnesium Alloy via Ultrasonic Surface Rolling Process. Advanced Engineering Materials, 2021, 23, 2100076.	3.5	8
13	Effect of AgNP distribution on the cotton fiber on the durability of antibacterial cotton fabrics. Cellulose, 2021, 28, 9489-9504.	4.9	12
14	Rapid nanowelding of silver nanowires by focused-light-scanning for high-performance flexible transparent electrodes. Nanotechnology, 2021, 32, 505208.	2.6	2
15	Reactive Dyeing of Cationized Cotton Fabric: The Effect of Cationization Level. ACS Sustainable Chemistry and Engineering, 2021, 9, 12355-12364.	6.7	21
16	Retarding Ostwald ripening through Gibbs adsorption and interfacial complexions leads to high-performance SnTe thermoelectrics. Energy and Environmental Science, 2021, 14, 5469-5479.	30.8	67
17	Russian-Doll-Like Molecular Cubes. Journal of the American Chemical Society, 2021, 143, 2537-2544.	13.7	44
18	FeS2 nanoparticles embedded in N/S co-doped porous carbon fibers as anode for sodium-ion batteries. Chemical Engineering Journal, 2020, 380, 122455.	12.7	129

#	Article	IF	CITATIONS
19	Efficient and Exponential Rolling Circle Amplification Molecular Network Leads to Ultrasensitive and Label-Free Detection of MicroRNA. Analytical Chemistry, 2020, 92, 2074-2079.	6.5	52
20	Target-dependent dual strand extension recycling amplifications for non-label and ultrasensitive sensing of serum microRNA. Talanta, 2020, 210, 120651.	5.5	4
21	Polymerization nicking-triggered LAMP cascades enable exceptional signal amplification for aptamer-based label-free detection of trace proteins in human serum. Analytica Chimica Acta, 2020, 1098, 164-169.	5.4	12
22	Dataset of full-length transcriptome assembly and annotation of apocynum venetum using pacbio sequel II. Data in Brief, 2020, 33, 106494.	1.0	4
23	Fabrication of high strength and plasticity of Zn-Mg composites with core–shell structure by spark plasma sintering. Materials Letters, 2020, 279, 128525.	2.6	8
24	FeS2@TiO2 nanorods as high-performance anode for sodium ion battery. Chinese Journal of Chemical Engineering, 2020, 28, 2699-2706.	3.5	17
25	Assembly properties of bacterial tubulin homolog FtsZ regulated by the positive regulator protein ZipA and ZapA from Pseudomonas aeruginosa. Scientific Reports, 2020, 10, 21369.	3.3	4
26	Interface characteristics of high-entropy alloy/Al-Mg composites by underwater friction stir processing. Materials Letters, 2020, 275, 128200.	2.6	10
27	High-performance p-type elemental Te thermoelectric materials enabled by the synergy of carrier tuning and phonon engineering. Journal of Materials Chemistry A, 2020, 8, 12156-12168.	10.3	12
28	Shielding composites for neutron and gamma-radiation with Gd2O3@W core-shell structured particles. Materials Letters, 2020, 276, 128082.	2.6	18
29	Charge compensation weakening ionized impurity scattering and assessing the minority carrier contribution to the Seebeck coefficient in Pb-doped Mg ₃ Sb ₂ compounds. Physical Chemistry Chemical Physics, 2020, 22, 7012-7020.	2.8	10
30	FeS2@C nanorods embedded in three-dimensional graphene as high-performance anode for sodium-ion batteries. Frontiers of Materials Science, 2020, 14, 255-265.	2.2	11
31	Surface modification of aluminum alloy by incorporation of AlCoCrFeNi high entropy alloy particles via underwater friction stir processing. Surface and Coatings Technology, 2020, 385, 125438.	4.8	28
32	Synergetic effect of interface barrier and doping on the thermoelectric transport properties of tellurium. Journal of Materials Science, 2020, 55, 8642-8650.	3.7	3
33	Reversal of prolonged obesity-associated cerebrovascular dysfunction by inhibiting microglial Tak1. Nature Neuroscience, 2020, 23, 832-841.	14.8	22
34	Densification of pure magnesium by spark plasma sintering-discussion of sintering mechanism. Advanced Powder Technology, 2019, 30, 2649-2658.	4.1	25
35	Hot Deformation and Processing Maps of B4C/6061Al Nanocomposites Fabricated by Spark Plasma Sintering. Journal of Materials Engineering and Performance, 2019, 28, 6287-6297.	2.5	6
36	Comparison of the Microstructure of M2 Steel Fabricated by Continuous Casting and with a Sand Mould. Metals, 2019, 9, 560.	2.3	5

#	Article	IF	CITATIONS
37	Alantolactone induces apoptosis through ROS-mediated AKT pathway and inhibition of PINK1-mediated mitophagy in human HepG2 cells. Artificial Cells, Nanomedicine and Biotechnology, 2019, 47, 1961-1970.	2.8	32
38	Interfacial characteristics and nano-mechanical properties of dissimilar 304 austenitic stainless steel/AZ31B Mg alloy welding joint. Journal of Manufacturing Processes, 2019, 42, 257-265.	5.9	18
39	Therapeutic Delivery of miR-29b Enhances Radiosensitivity in Cervical Cancer. Molecular Therapy, 2019, 27, 1183-1194.	8.2	27
40	Interfacial microstructure evolution and deformation mechanism in an explosively welded Al/Mg alloy plate. Journal of Materials Science, 2019, 54, 9155-9167.	3.7	14
41	Bright Alloy CdZnSe/ZnSe QDs with Nonquenching Photoluminescence at High Temperature and Their Application to Light-Emitting Diodes. Journal of Nanomaterials, 2019, 2019, 1-8.	2.7	6
42	Microstructure, mechanical, corrosion properties and cytotoxicity of beta‑calcium polyphosphate reinforced ZK61 magnesium alloy composite by spark plasma sintering. Materials Science and Engineering C, 2019, 99, 1035-1047.	7.3	45
43	Shikonin induces apoptosis and prosurvival autophagy in human melanoma A375 cells via ROS-mediated ER stress and p38 pathways. Artificial Cells, Nanomedicine and Biotechnology, 2019, 47, 626-635.	2.8	72
44	Characterization of the complete chloroplast genome sequence of <i>Pinus pumila</i> (Pinaceae). Mitochondrial DNA Part B: Resources, 2019, 4, 290-291.	0.4	3
45	Assembly properties of the bacterial tubulin homolog FtsZ from the cyanobacterium Synechocystis sp. PCC 6803. Journal of Biological Chemistry, 2019, 294, 16309-16319.	3.4	7
46	SURFACE-MODIFIED SEPIOLITE NANOFIBERS AS A NOVEL LUBRICANT ADDITIVE. Clays and Clay Minerals, 2019, 67, 283-290.	1.3	2
47	Ultrasonic effect mechanism on transient liquid phase bonding joints of SiCp reinforced Mg metal matrix composites using Zn-Al-Zn multi-interlayer. Ultrasonics Sonochemistry, 2018, 43, 101-109.	8.2	11
48	Microstructure and mechanical properties of Ni-Cr-Si-B-Fe composite coating fabricated through laser additive manufacturing. Journal of Alloys and Compounds, 2018, 747, 401-407.	5.5	22
49	Microstructure and thermal shock behavior of sol–gel introduced ZrB2 reinforced SiBCN matrix. Journal of Sol-Gel Science and Technology, 2018, 86, 365-373.	2.4	6
50	lsotropic Mg3Sb2 compound prepared by solid-state reaction and ball milling combined with spark plasma sintering. Journal of Materials Science, 2018, 53, 8039-8048.	3.7	9
51	Thermoelectric Properties and Transport Mechanism of Pure and Biâ€Doped SiNWsâ€Mg ₂ Si. Physica Status Solidi (A) Applications and Materials Science, 2018, 215, 1700742.	1.8	6
52	The dynamic properties of B ₄ C/6061Al neutron absorber composites fabricated by power metallurgy. Materials Science and Technology, 2018, 34, 504-512.	1.6	8
53	Microstructure evolution and mechanical properties of an AA6061/AZ31B alloy plate fabricated by explosive welding. Journal of Alloys and Compounds, 2018, 735, 1759-1768.	5.5	96
54	Microstructure and Mechanical Properties of B ₄ C/6061Al Nanocomposites Fabricated by Advanced Powder Metallurgy. Advanced Engineering Materials, 2018, 20, 1701133.	3.5	8

#	Article	IF	CITATIONS
55	Deformation behaviors and cyclic strength assessment of AZ31B magnesium alloy based on steady ratcheting effect. Materials Science & Engineering A: Structural Materials: Properties, Microstructure and Processing, 2018, 723, 212-220.	5.6	292
56	A simple approach for glutathione functionalized persistent luminescence nanoparticles as versatile platforms for multiple <i>in vivo</i> applications. Chemical Communications, 2018, 54, 3504-3507.	4.1	18
57	Metal–Organic Framework-Derived Sea-Cucumber-like FeS ₂ @C Nanorods with Outstanding Pseudocapacitive Na-Ion Storage Properties. ACS Applied Energy Materials, 2018, 1, 6234-6241.	5.1	47
58	Ratcheting Strain and Microstructure Evolution of AZ31B Magnesium Alloy under a Tensile-Tensile Cyclic Loading. Materials, 2018, 11, 513.	2.9	10
59	Microstructure and Corrosion Resistance of Laser-Welded Crossed Nitinol Wires. Materials, 2018, 11, 842.	2.9	7
60	Numerical study on the interfacial behavior of Mg/Al plate in explosive/impact welding. Science and Engineering of Composite Materials, 2017, 24, 581-590.	1.4	16
61	Numerical study of Ti/Al/Mg three-layer plates on the interface behavior in explosive welding. Science and Engineering of Composite Materials, 2017, 24, 833-843.	1.4	10
62	Elevated electrochemical corrosion behavior of a B4C/Al neutron absorber by shot peening modification. Science and Engineering of Composite Materials, 2017, 24, 547-556.	1.4	1
63	Influence of hot rolling on the interface microstructure and mechanical properties of explosive welded Mg/Al composite plates. Journal of Materials Research, 2017, 32, 863-873.	2.6	15
64	DiffusionÂbonding of Ti/Ni under the influence ofÂanÂelectricÂcurrent: mechanism and bond structure. Journal of Materials Science, 2017, 52, 3535-3544.	3.7	15
65	Effect of plastic anisotropy of ZK60 magnesium alloy sheet on its forming characteristics during deep drawing process. International Journal of Advanced Manufacturing Technology, 2017, 88, 1629-1637.	3.0	8
66	Preparation of Mg/Nanoâ€HA Composites by Spark Plasma Sintering Method and Evaluation of Different Milling Time Effects on Their Microhardness, Corrosion Resistance, and Biocompatibility. Advanced Engineering Materials, 2017, 19, 1600294.	3.5	11
67	A Method for Identifying the Mood States of Social Network Users Based on Cyber Psychometrics. Future Internet, 2017, 9, 22.	3.8	5
68	Dramatically enhanced impact toughness in welded ultra-ferritic stainless steel by additional nitrogen gas in Ar-based shielding gas. Journal of Materials Research, 2016, 31, 3610-3618.	2.6	7
69	An experimental study of nitrogen gas influence on the 443 ferritic stainless steel joints by double-shielded welding. International Journal of Advanced Manufacturing Technology, 2016, 87, 3315-3323.	3.0	5
70	CD/AuNPs/MWCNTs based electrochemical sensor for quercetin dual-signal detection. Biosensors and Bioelectronics, 2016, 77, 638-643.	10.1	50
71	Treatment of pharmaceutical wastewater using interior micro-electrolysis/Fenton oxidation-coagulation and biological degradation. Chemosphere, 2016, 152, 23-30.	8.2	88
72	A multiproxy analysis of sedimentary organic carbon in the <scp>Changjiang Estuary</scp> and adjacent shelf. Journal of Geophysical Research G: Biogeosciences, 2015, 120, 1407-1429.	3.0	74

#	Article	IF	CITATIONS
73	Historical reconstruction of organic carbon inputs to the East China Sea inner shelf: Implications for anthropogenic activities and regional climate variability. Holocene, 2015, 25, 1869-1881.	1.7	24
74	A prostate cancer-targeted polyarginine-disulfide linked PEI nanocarrier for delivery of microRNA. Cancer Letters, 2015, 365, 156-165.	7.2	68
75	The effect of annealing on the interface microstructure and mechanical characteristics of AZ31B/AA6061 composite plates fabricated by explosive welding. Materials & Design, 2015, 65, 1100-1109.	5.1	131
76	HAF drives the switch of HIF-1α to HIF-2α by activating the NF-κB pathway, leading to malignant behavior of T24 bladder cancer cells. International Journal of Oncology, 2014, 44, 393-402.	3.3	35
77	A Nearâ€Infrared Lightâ€Triggered Nanocarrier with Reversible DNA Valves for Intracellular Controlled Release. Advanced Functional Materials, 2013, 23, 2255-2262.	14.9	91
78	Laser cladding Al-Si/Al2O3-TiO2 composite coatings on AZ31B magnesium alloy. Journal Wuhan University of Technology, Materials Science Edition, 2012, 27, 1042-1047.	1.0	7
79	Preparation, Morphology and Properties of Electrospun Lauric Acid/PET Form-Stable Phase Change Ultrafine Composite Fibres. Polymers and Polymer Composites, 2011, 19, 773-780.	1.9	14
80	As-extruded AZ31B magnesium alloy fatigue crack propagation behavior. Journal Wuhan University of Technology, Materials Science Edition, 2011, 26, 1114-1120.	1.0	3
81	Direct electrocatalytic reduction of hydrogen peroxide at a glassy carbon electrode modified with polypyrrole nanowires and platinum hollow nanospheres. Mikrochimica Acta, 2010, 171, 125-131.	5.0	43
82	A Novel Nonenzymatic Hydrogen Peroxide Sensor Based on a Polypyrrole Nanowire-Copper Nanocomposite Modified Gold Electrode. Sensors, 2008, 8, 5141-5152.	3.8	63